TITLE

FIRST AND SECOND ORDER SIMPLIFIED MODELS FOR THE PERFORMANCE EVALUATION OF LOW TEMPERATURE ACTIVATED DESICCANT WHEELS

Authors: F. Comino [a], M. Ruiz de Adana [a], F. Peci [a], M. Zamora [b]

[a] Departamento de Química-Física y Termodinámica Aplicada, Escuela Politécnica Superior, Universidad de Córdoba, Campus de Rabanales, Antigua Carretera Nacional IV, km 396, 14072 Córdoba, Spain

[b] CIAT, Departamento de I+D+i. Pol. Llanos de Jarata s/n. 14550 Montilla, Córdoba, Spain

ABSTRACT

Hybrid systems with desiccant wheel, DW, are an alternative to conventional heating, ventilation and air conditioning, HVAC, systems for dehumidification and humidity control in rooms with high latent loads. The objective of this study was to obtain a DW model which represents accurately the behaviour of a DW activated at low temperature

For this, the statistical design of experiments technique, DOE, was used to obtain first and second order simplified models to analyze the behaviour of DW's in low temperature activated hybrid systems. The proposed models can be used to predict the influence of the inlet process air and inlet regeneration air, on the air process outlet temperature and humidity ratio.

The proposed methodology showed that a reduced number of experimental tests are required to fit the mathematical model. The accuracy of the numerical results of the mathematical models were acceptable, with maximum deviations below 4% for temperature and 10% for humidity ratio. The second order model was considered to be the best option due to the balance between accuracy and low number of experimental tests.

The results showed a significant influence of the inlet humidity ratio of the air process and regeneration on the increase of the dehumidification ratio.

Keywords: desiccant wheel; low temperature activated systems; design of experiments

Nomenclature

a	estimated parameter
CC	cooling coil
DOE	design of experiments
DW	desiccant wheel
EA	exhaust air
F	centrifugal fan
FC	flow conditioner
EH	electric heater
HC	heating coil
HR	relative humidity [%]
k	number of parameters
MA	mixed air
MB	mixing box
N	number of design experimental tests
OA	outdoor air
PT	pitot tube
RA	recirculated air
$RMSE_T$	root mean square error for temperature [ºC]
$RMSE_\omega$	root mean square error for temperature [g kg^{-1}]
SH	steam humidifier
T	temperature [ºC]
X	input variable
$\hat{Y}$	estimated output value
Greek letters	
ΔP	pressure difference [Pa]
δT	error in predicting the temperature variation of the process air [%]
$\delta\omega$	error in predicting the humidity ratio variation of the process air [%]
ω	humidity ratio [g kg^{-1}]
Ω	specific mass airflow rate [kg s^{-1} m^{-3}]
Subscripts	
num	simulated values of temperature or humidity ratio
d	dew point
exp	experimental values of temperature or humidity ratio
i	inlet
o	outlet
p	process
r	regeneration

1 INTRODUCTION

The control of the water vapour content in the air is necessary to maintain the required indoor conditions for thermal comfort of certain industrial processes. The external and internal latent

loads in a room can produce an increase of water vapour, so it is necessary to use a system to reduce and control the humidity ratio. Some examples of local high latent loads are restaurants, indoor swimming pools or spas. Traditional HVAC systems, with cooling dehumidifiers, usually control comfort conditions in a room, but these systems present problems when simultaneously controlling sensible and latent loads [1]. Hybrid systems based on combinations of traditional systems with desiccant wheels can be an alternative to solve this problem. In these systems the space latent and sensible loads are decoupled [2]. Hybrid systems can operate with low values of sensible heat factor, which are particularly suitable for rooms with high latent loads. Desiccant dehumidifiers differ from cooling dehumidifiers in the way of removing water from the humid air stream. Instead of cooling the air to condense its moisture, desiccants attract moisture from the air by creating an area of low vapour pressure at the surface of the desiccant. The pressure exerted by the water in the air is higher, so the water molecules move from the air to the desiccant and the air is dehumidified [3]. Furthermore, desiccants can retain substances other than water vapour, these allow removing contaminants from the air stream for improving the indoor air quality in buildings [4].

Many studies about hybrid systems with desiccant wheels, DW, have been carried out [5–8]. Energy savings were obtained only when the DW was regenerated using waste heat from another process. Some authors studied the behaviour of hybrid systems using waste energy to regenerate the DW, obtaining great economic savings [8–10]. However, in some cases either waste heat energy is not available or the corresponding temperature level is not adequate. In recent years, some studies have analysed the use of solar energy to regenerate DW's [6,7]. However, these systems required an auxiliary source of heat. The solar system also involved a significant increase in the overall system economic cost.

A DW integrated in a hybrid system can be operated at low regeneration temperatures. Hybrid systems with temperatures of air of regeneration of 55°C and 46ºC [9,11] has been analyzed, showing acceptable desiccant capacity. Two low temperature activated systems with DW are shown in Fig. 1. The first system is composed of a solar heating system and a low temperature boiler that supplies hot water to the heating coil, HC. The HC heats up the regeneration air

previous to the DW, see Fig. 1a. Fig. 1b shows a low regeneration temperature hybrid system composed by a refrigeration vapour compression system and DW. This hybrid system allows the regeneration of the DW using the heat from the condenser. In addition, the evaporator cooling effect is used to cool and dehumidify the process air.

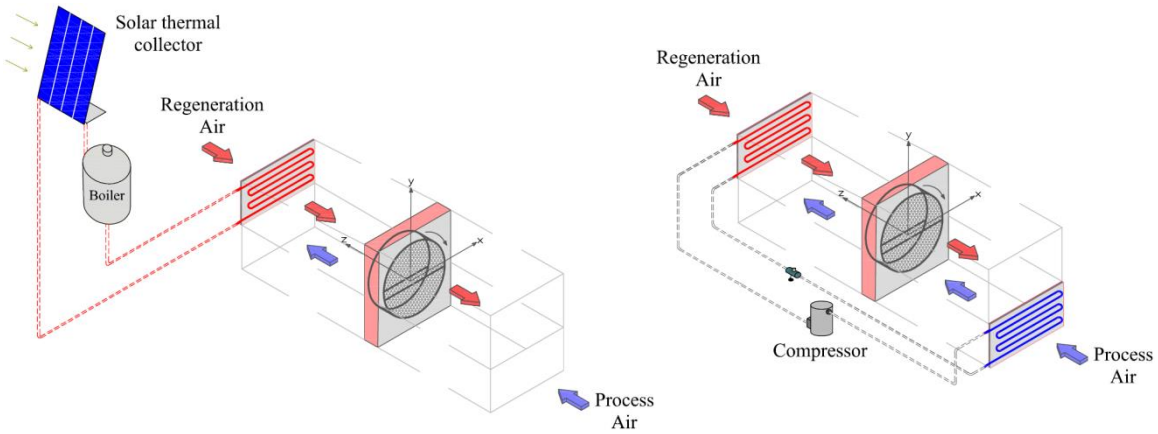

Fig. 1. Schematic of low temperature activated systems (a) solar thermal system with desiccant wheel; (b) hybrid refrigeration system with desiccant wheel.

A numerical model of a DW is very convenient for parametric optimization analysis of hybrid systems. Different experimental and numerical research works have been carried out for the characterization of the operating parameters that influence the overall performance of the DW. Some researchers developed detailed models, considering the heat and mass transfer in the DW [12–16]. These models are not easy to implement and require high computation time. Moreover, some constructive parameters and materials data of the DW are not normally available.

Another modelling approach is based on simplified models of the DW which require less computation time. A widely used simplified method to study the behaviour of the DW is that based on the effectiveness concept. It is also referred to as the linear analogy method [17] and takes into account two independent potential variables [18]. The effectiveness method based on constant values has been used previously in several studies [19,20]. Simplified mathematical models are easy to implement, but many experimental tests are needed to fit the effectiveness parameters in the model. Important errors can be introduced when constant values of the

effectiveness parameters are assumed in the effectiveness method [21]. Simplified mathematical models can be improved by using variable parameters of efficiency. However, the accuracy of simplified models is reduced when variable parameters of efficiency are obtained by means of interpolation [21].

Other authors have developed empirical correlations to study the behaviour of the wheel [22,23]. The advantage of this approach is that the model fits the constructive characteristics and specific materials of a DW. However the empirical model obtained can not be used in a different DW from that in which it was obtained.

This work aims at obtaining a DW model which represents accurately the behaviour of a DW activated at low temperature. The methodology used is based on the statistical technique of design of experiments, DOE, which allows to fit the DW model with a reduced number of experimental tests. A DW model can be helpful to identify the most influential factors in the behaviour of systems with low regeneration temperatures.

2 METHODOLOGY

2.1 Experimental setup

A schematic diagram of the DW experimental setup is shown in Fig. 2. Process and regeneration air streams were arranged in counterflow in independent ducts. Inlet process air and regeneration air conditions were generated by means of cooling coil, CC, heating coil, HC, electric heater, EH, and a steam humidifier, SH, that were installed for each air steam upstream to the DW [24,25]. The process and regeneration air flow rates were controlled by means of variable speed fans. Two mixing boxes allowed recirculation of process and regeneration air streams or to mix the outdoor air with the treated air. These devices provided the required conditions of temperature, humidity and airflow rate at the process and regeneration inlets of the DW. Characteristic of the equipment of the experimental test rig setup are shown in Table 1.

Table 1. Characteristics of equipment.

Equipment	Value

Cooling coil (CC)		
Total cooling capacity	15.8	[kW]
Sensible cooling capacity	12.2	[kW]
Nominal water flow	2.7	[m^3 h^{-1}]
Pressure drop	5.1	[m]
Heating coil (HC)		
Heating capacity	18.8	[kW]
Nominal water flow	2.7	[m^3 h^{-1}]
Pressure drop	5.1	[m]
Electric heater (EH)		
Electric power	7.2	[kW]
Fan (F)		
Nominal airflow	3100	[m^3 h^{-1}]
Available static pressure	0.007	[m]
Nominal motor power	0.6	[kW]
Speed	1125	[rpm]
Steam humidifier (SH)		
Steam flow	45	[kg h^{-1}]
Max. power	33.75	[kW]

The DW was enclosed in a steel cassette and it was driven by a constant speed motor at 42 rph. The matrix of the DW consisted of alternate layers of flat and corrugated sheets of silica gel and metal silicates, chemically bonded into a tissue of inorganic fibres. The process and regeneration streams lay-out was 50% process-50% regeneration. Other characteristics of the DW are shown in Table 2.

Table 2. Characteristics of desiccant wheel.

Parameters	Value	
Rotor diameter	550	[mm]
Rotor length	200	[mm]
Desiccant material	Silica gel	
Channel shape	Honeycomb	
Nominal capacity	15	[kg h^{-1}]
Nominal air flow	2300	[m^3 h^{-1}]
Rotation speed	42	[rph]
Weight	57	[kg]
Power supply	230	[V]

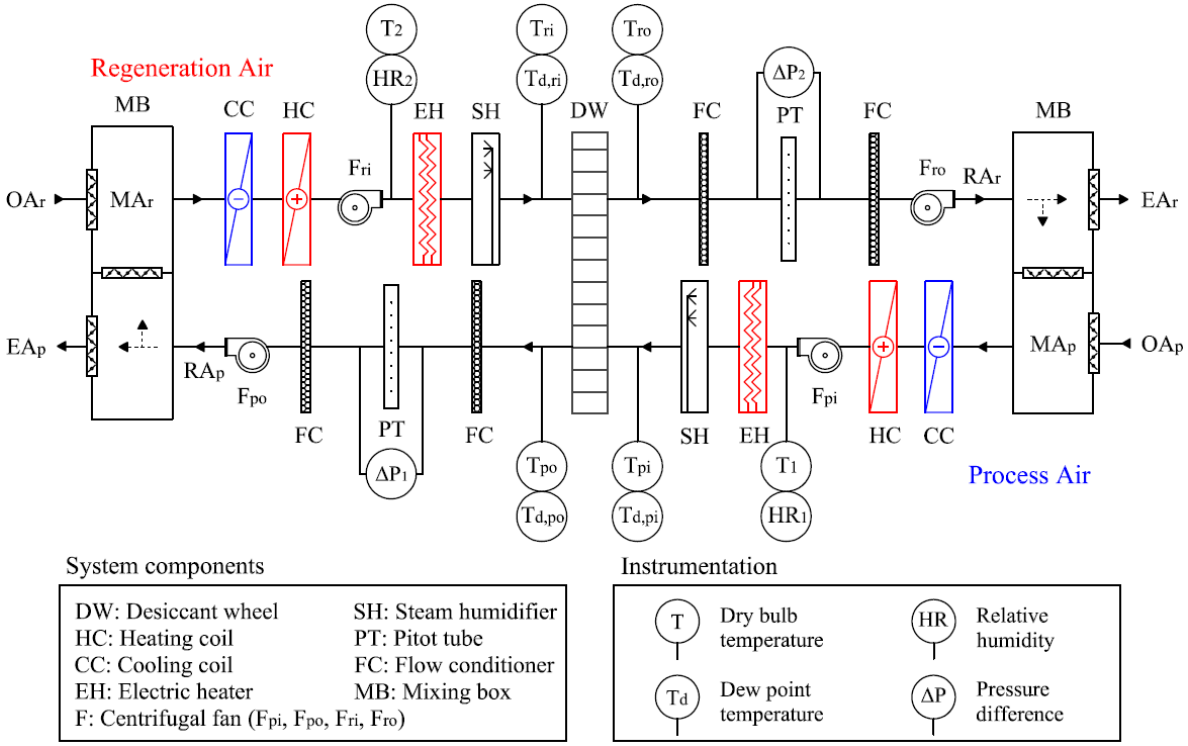

Fig. 2. Lay-out of test facility.

The measurement of air flow rate was performed with two averaging Pitot tubes, PT. In order to obtain a stable airflow, four flow conditioners, FC, were installed in the ducts, two upstream the air flow rate measuring point and two downstream.

The measured variables in the test rig, the type of sensor and its accuracy are shown in Table 3. The locations of the sensors are showed in Fig. 2. The temperatures and humidities at the inlet and outlet of the DW were measured at three different points of the horizontal axis, averaging the three measurements [26]. All the experimental tests were carried out under steady state conditions. The sampling time was 3 s and the values were averaged every 20 min.

Table 3. Specification of measuring devices.

Measured parameter	Type	Accuracy
T_1, T_2, T_{pi}, T_{po}, T_{ri}, T_{ro}	PT 100	± 0.12 ºC
$T_{d,pi}$, $T_{d,po}$	Chilled mirror hygrometer	± 0.15 ºC
$T_{d,ri}$, $T_{d,ro}$	Capacitive	± 0.4 ºC
HR_1, HR_2	Capacitive	± 3 %
ΔP_1, ΔP_2	Differential pressure transmitter	± 0.3 % (0 to 1 mbar)

2.2 Design of experiment

The statistical technique DOE was used to fit different models with the experimental data. DOE is a methodology to systematically apply Statistics to the process of experimental tests [27,28].

Three cases were studied using different inputs and outputs variables, as shown in Table 4. The considered inputs variables were the inlet air process temperature, T_{pi}, inlet air process humidity ratio, ω_{pi}, process specific mass airflow rate, Ω_p, ratio of inlet mass velocity to the channel length [21], inlet air regeneration temperature, T_{ri}, inlet air regeneration humidity ratio, ω_{ri}, and regeneration specific mass airflow rate, Ω_r. The considered output variables were the outlet air process temperature, T_{po}, and outlet air process humidity ratio, ω_{po}. In case studies 1 and 3, the effect of four input variables, T_{pi}, ω_{pi}, T_{ri}, ω_{ri}, was studied considering a two level factorial design [27] and a three level box-Behnken design [27], respectively. In case study 2, the effect of five input variables, T_{pi}, ω_{pi}, T_{ri}, ω_{ri}, Ω_p, Ω_r, was studied considering a two level factorial design. Both air streams were considered balanced for all cases.

Table 4. Case studies of design of experiments.

Case study	Type design	Order	Input variables						Output variables	
			T_{pi}	ω_{pi}	T_{ri}	ω_{ri}	Ω_p	Ω_r	T_{po}	ω_{po}
1	2 level factorial	First	x	x	x	x			x	x
2	2 level factorial	First	x	x	x	x	x	x	x	x
3	3 level box-Behnken	Second	x	x	x	x			x	x

2.2.1 Case study 1

Two grids were defined to cover the range of validity of the process and regeneration air streams, as shown in Fig. 3. The ranges were selected to implement the DW model in low temperature activated hybrid models.

The DOE methodology starts defining a grid: (i) four different inlet states for the process airflow were selected, P1 to P4, as showed in the psychrometric chart of Fig. 3, covering the range of interest, (ii) a fifth inlet state P5 was added, located inside the four-sided polygon previously created. The regeneration inlet condition can be treated in the same manner,

introducing another set of five points R1 to R5, see Fig. 3. The conditions P1-P4 of the inlet states for the process airflow were combined with the conditions R1-R4 of the inlet states for the regeneration airflow, to study the behaviour of the input variables. The interior points P5 and R5 were combined to obtain the independent estimate of experimental error. The resulted process grid was not rectangular, in order to obtain the widest range of validity. The inlet states used for each input variables are shown in

Table 5. All the tests were performed using the nominal air flow rate of the DW. The study consisted of 19 experimental tests, including 3 replicates of the tests combining the interior points, and 8 degrees of freedom. The results of this set of experiments were used to fit the parameters of a first order model expressed by the Eq. (1):

$$\hat{Y} = a_0 + \sum_{i=1}^{k} a_i \cdot X_i \qquad (1)$$

Where k is the number of parameters, a_0 and a_i are the estimated parameters, X are input variables and $\hat{Y}$ is the estimated output value.

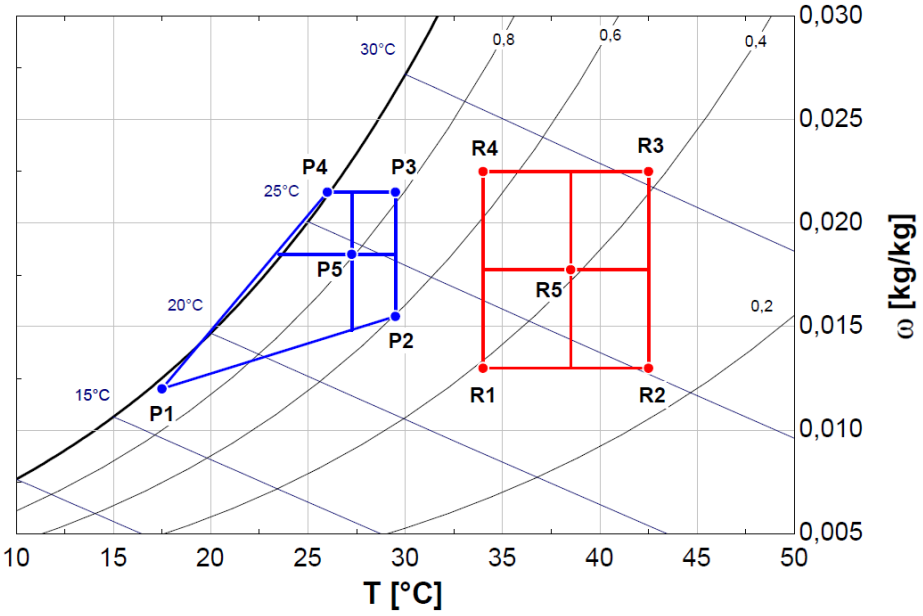

Fig. 3. Grid considered for the inlet states of the process and regeneration airflow for case studies 1 and 2.

Table 5. Inlet states airflow for case studies 1 and 2.

Point	T_{pi} [ºC]	ω_{pi} [g kg^{-1}]	Point	T_{ri} [ºC]	ω_{ri} [g kg^{-1}]
P1	17.50	12.00	R1	34.00	13.00
P2	29.50	15.50	R2	42.50	13.00
P3	29.50	21.50	R3	42.50	22.50
P4	26.00	21.50	R4	34.00	22.50
P5	27.25	18.50	R5	38.50	17.75

2.2.2 Case study 2

The same grids as in case 1 were used in case study 2, see Fig. 3. The values of temperature and humidity ratio were the same as in case 1, as shown in

Table 5. The specific mass airflow rate range considered varied from 14.79 kg s^{-1} m^{-3} to 30.92 kg s^{-1} m^{-3}. A total of 35 experimental tests were carried out, including 3 replicates of the tests combining the interior points, and 16 degrees of freedom. The results of this set of experiments were used to fit the parameters of a model expressed by the Eq. (1).

2.2.3 Case study 3

Two grids were defined, to cover the same range of validity as cases 1 and 2, but with additional inlet states, see Fig. 4. The two grids were defined by different inlet states for process air inlet, P1-P9, and inlet states for regeneration air inlet, R1-R9. The inlet states P1-P4 of the process air were combined with the regeneration interior point, R5. The inlet states R1-R4 of the regeneration air were combined with the process interior point, P5. The inlet states P6-P9 were combined with the inlet states R6-R9. Finally, the interior points P5 and R5 were combined to obtain the independent estimate of experimental error. The considered inlet states for each input variable are shown in Table 6. All the tests were performed for nominal air flow rate of the DW. There were a total of 27 experimental tests, including 3 replicates of the tests combining the interior points, and 12 degrees of freedom. The results of this set of experiments were used to fit the parameters of a second order model expressed by the Eq. (2):

$$\hat{Y} = a_0 + \sum_{i=1}^{k} a_i \cdot X_i + \sum_{i=1}^{k} a_{ii} \cdot X_i^2 + \sum_{i=1}^{k=1} \sum_{\substack{i=2 \\ j>i}}^{k} a_{ij} \cdot X_i \cdot X_j \qquad (2)$$

Where k is number of parameters, a_0 and a_i are the estimated parameters, X are input variables and $\hat{Y}$ is the estimated output value.

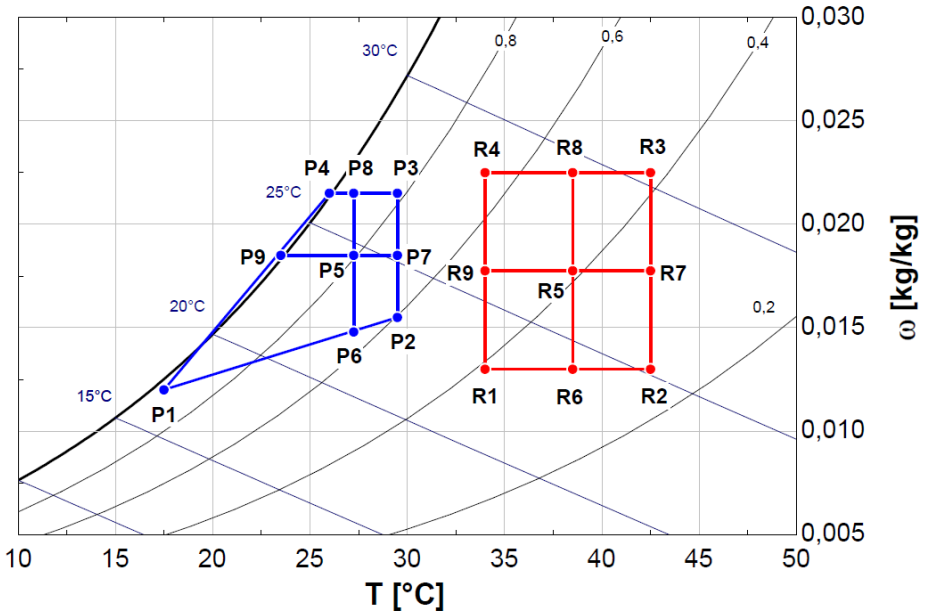

Fig. 4. Grid considered for the inlet states of the process and regeneration airflow for case study 3.

Table 6. Inlet states airflow for case study 3.

Point	T_{pi} [ºC]	ω_{pi} [g kg^{-1}]	Point	T_{ri} [ºC]	ω_{ri} [g kg^{-1}]
P1	17.50	12.00	R1	34.00	13.00
P2	29.50	15.50	R2	42.50	13.00
P3	29.50	21.50	R3	42.50	22.50
P4	26.00	21.50	R4	34.00	22.50
P5	27.25	18.50	R5	38.50	17.75
P6	27.25	14.60	R6	38.50	13.00
P7	29.50	18.50	R7	42.50	17.75
P8	27.25	21.50	R8	38.50	22.50
P9	24.00	18.50	R9	34.00	17.75

2.3 Validation of models

In order to have a quantitative estimation of the difference between experimental measured and simulated temperature and humidity ratio values, the root mean square error, RMSE, was calculated [20], using Eq. (3-4):

$$RMSE_T = \sqrt{\frac{\sum_{i=1}^{N}(T_{i,po,exp} - T_{i,po,num})^2}{N}} \quad (3)$$

$$RMSE_\omega = \sqrt{\frac{\sum_{i=1}^{N}(\omega_{i,po,exp} - \omega_{i,po,num})^2}{N}} \quad (4)$$

The experimental tests used to validate the models were different than those used to fit the models. All of them used data within the same range of validity. A psychrometric chart with the inlet states of the process air and regeneration air for the three case studies is shown in Fig. 5. A number of 30 validation experimental tests were carried out for case studies 1 and 3. A number of 50 validation experimental tests were carried out in the case study 2 to consider the influence of the specific mass airflow rate treated by the DW, where 30 tests coincided to the three case studies.

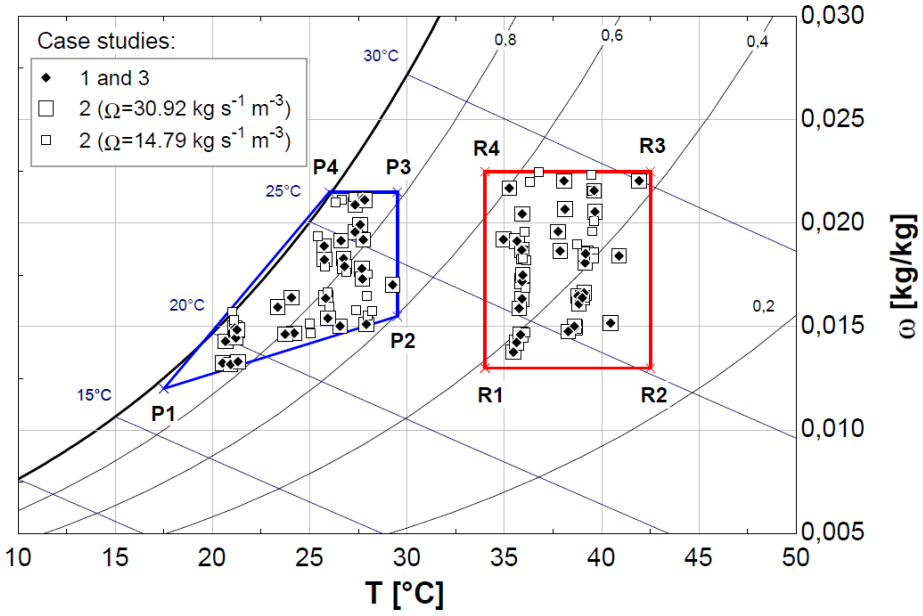

Fig. 5. Inlet states of the process air and regeneration air of the validation experimental tests.

3 RESULTS AND ANALYSIS

3.1 First and second order models

The output variables, outlet process temperature, T_{po}, and the outlet process humidity ratio, ω_{po}, can be calculated using Eq. (5) for the first order model of case study 1, Eq. (6) for the first order model of case study 2 and Eq. (7) for the second order model of case study 3. In Eq. (6) the input variable Ω corresponds to the specific mass airflow process flow, Ω_p, and the specific mass airflow regeneration, Ω_r.

$$\hat{Y} = a_0 + a_1 \cdot T_{pi} + a_2 \cdot \omega_{pi} + a_3 \cdot T_{ri} + a_4 \cdot \omega_{ri} + a_5 \cdot T_{pi} \cdot \omega_{pi} + a_6 \cdot T_{pi} \cdot T_{ri} + a_7 \cdot T_{pi} \cdot \omega_{ri} + a_8 \cdot \omega_{pi} \cdot T_{ri} + a_9 \cdot \omega_{pi} \cdot \omega_{ri} + a_{10} \cdot T_{ri} \cdot \omega_{ri} \quad (5)$$

$$\hat{Y} = a_0 + a_1 \cdot T_{pi} + a_2 \cdot \omega_{pi} + a_3 \cdot T_{ri} + a_4 \cdot \omega_{ri} + a_5 \cdot \Omega + a_6 \cdot T_{pi} \cdot \omega_{pi} + a_7 \cdot T_{pi} \cdot T_{ri} + a_8 \cdot T_{pi} \cdot \omega_{ri} + a_9 \cdot T_{pi} \cdot \Omega + a_{10} \cdot \omega_{pi} \cdot T_{ri} + a_{11} \cdot \omega_{pi} \cdot \omega_{ri} + a_{12} \cdot \omega_{pi} \cdot \Omega + a_{13} \cdot T_{ri} \cdot \omega_{ri} + a_{14} \cdot T_{ri} \cdot \Omega + a_{15} \cdot \omega_{ri} \cdot \Omega \quad (6)$$

$$\hat{Y} = a_0 + a_1 \cdot T_{pi} + a_2 \cdot \omega_{pi} + a_3 \cdot T_{ri} + a_4 \cdot \omega_{ri} + a_5 \cdot T_{pi}^2 + a_6 \cdot T_{pi} \cdot \omega_{pi} + a_7 \cdot T_{pi} \cdot T_{ri} + a_8 \cdot T_{pi} \cdot \omega_{ri} + a_9 \cdot \omega_{pi}^2 + a_{10} \cdot \omega_{pi} \cdot T_{ri} + a_{11} \cdot \omega_{pi} \cdot \omega_{ri} + a_{12} \cdot T_{ri}^2 + a_{13} \cdot T_{ri} \cdot \omega_{ri} + a_{14} \cdot \omega_{ri}^2 \quad (7)$$

Where the output variable $\hat{Y}$, correspond to the outlet process temperature, T_{po}, or the outlet process humidity ratio, ω_{po}. The corresponding estimated parameters are shown in Table 7.

Table 7. Estimated parameters for case studies.

Estimated parameters	Case study 1		Case study 2		Case study 3	
	T_{po} (x10^3) [ºC]	ω_{po} (x10^3) [g kg^{-1}]	T_{po} (x10^3) [ºC]	ω_{po} (x10^3) [g kg^{-1}]	T_{po} (x10^3) [ºC]	ω_{po} (x10^3) [g kg^{-1}]
a_0	6081.84	-16707.70	9012.70	-4828.58	93985.40	-9448.80
a_1	328.15	144.14	-25.41	-16.01	-177.97	1277.70
a_2	-400.65	1786.87	23.17	1783.16	-392.09	-1217.59
a_3	438.02	82.74	543.06	-189.88	-3168.40	82.29
a_4	-49.42	505.68	-291.07	485.12	-1361.45	1188.94

a_5	8.64	-19.08	-26.53	-337.70	-8.35	-44.00
a_6	3.49	3.80	6.38	-7.31	-17.27	78.95
a_7	-1.91	2.16	7.34	7.44	28.64	9.202
a_8	4.62	-6.52	-2.36	8.74	21.52	-28.54
a_9	9.73	-13.22	8.41	-8.42	30.12	-10.47
a_{10}	-6.78	-4.24	-0.21	-20.09	-8.06	-11.85
a_{11}	-	-	4.78	-11.79	11.17	29.96
a_{12}	-	-	3.04	6.25	37.53	-2.63
a_{13}	-	-	-0.51	-4.71	7.06	-5.08
a_{14}	-	-	-7.56	14.04	5.39	-14.74
a_{15}	-	-	3.31	-5.11	-	-

3.2 Statistical analysis.

The results of the analyses of variance, ANOVA, for the three case~~s~~ studies are summarized in Table 8. It is shown each of the main estimated effects, the standard error of each of the effects, which measures their sampling error, the statistical parameter F-Ratio, the statistical parameter P-value and the lack of fit test. All variables were found significant at 95% confidence level. Therefore, a variation of the output variables with the input variables was expected. The models were found suitable for the observed data at 95 % confidence level, since the P-values for lack-of-fit tests were greater to 0.05 in all cases.

The results for the case studies 1 and 3 showed that the most influential variables on the outlet process temperature, T_{po}, sorted from most to least influential, were: regeneration inlet air temperature, T_{ri}, process inlet air temperature, T_{pi}, inlet regeneration humidity ratio, ω_{ri}, and inlet process humidity ration, ω_{pi}, as a result of the parameter P-value. Regarding outlet process humidity ratio, ω_{po}, the most influential variables, sorted from most to least influential, were: inlet process humidity ratio, ω_{pi}, inlet regeneration humidity ratio, ω_{ri}, inlet regeneration air temperature, T_{ri}, and inlet process air temperature, T_{pi}, as a result of the parameter P-value. This suggested that, if extremely dry process air outlet conditions were necessary, the inlet regeneration humidity ratio, ω_{ri}, should not be very high, and if low temperature air outlet conditions were necessary, the regeneration temperature, T_{ri}, should not be high.

The results for the case study 2 showed that the temperature, humidity ratio and specific mass airflow rate of the process air and regeneration air were influential to the output variables. This indicated that, if the moisture loading of the desiccant increased, it would be important to keep

the process and regeneration airflow in proportion to the moisture load being absorbed by the desiccant on the process air side. However, to achieve greater dehumidification, the specific mass airflow rates were less influential than the inlet process and regeneration air temperatures and humidity ratios, according to the parameter P-value.

Table 8. Effects of input variables on output variables of the DW.

Case study 1								
	T_{po}				ω_{po}			
Effect	Estimate	Stnd. Error	F-Ratio	P-value	Estimate	Stnd. Error	F-Ratio	P-value
Average	29.96	0.12			14.21	0.05		
T_{pi}	4.05	0.28	594.24	0.0017	-0.69	0.17	22.12	0.0450
ω_{pi}	1.44	0.23	38.74	0.0249	7.64	0.16	2326.64	0.0004
T_{ri}	6.87	0.12	997.45	0.0010	0.78	0.1	23.20	0.0405
ω_{ri}	-1.81	0.12	198.85	0.0050	1.58	0.1	248.43	0.0040
	Lack-of-fit P-value: 0.102				Lack-of-fit P-value: 0.097			
Case study 2								
	T_{po}				ω_{po}			
Effect	Estimate	Stnd. Error	F-Ratio	P-value	Estimate	Stnd. Error	F-Ratio	P-value
Average	31.33	0.04			14.64	0.04		
T_{pi}	4.53	0.08	4542.12	0.0002	-1.01	0.08	161.79	0.0061
ω_{pi}	1.96	0.07	1935.40	0.0006	7.64	0.07	11789.5	0.0001
T_{ri}	5.89	0.04	13011.2	0.0001	1.08	0.04	688.45	0.0014
ω_{ri}	-2.01	0.04	2559.92	0.0004	1.88	0.04	2357.63	0.0004
Ω	-1.45	0.04	744.94	0.0013	0.24	0.04	40.54	0.0238
	Lack-of-fit P-value: 0.072				Lack-of-fit P-value: 0.102			
Case study 3								
	T_{po}				ω_{po}			
Effect	Estimate	Stnd. Error	F-Ratio	P-value	Estimate	Stnd. Error	F-Ratio	P-value
Average	29.47	0.07			14.97	0.07		
T_{pi}	2.99	0.49	203.35	0.0049	-1.51	0.19	99.48	0.0099
ω_{pi}	1.24	0.23	29.31	0.0325	3.75	0.10	1416.55	0.0007
T_{ri}	7.05	0.17	310.53	0.0032	1.98	0.12	170.63	0.0058
ω_{ri}	-1.78	0.17	110.22	0.0090	2.36	0.12	417.13	0.0024
	Lack-of-fit P-value: 0.085				Lack-of-fit P-value:0.099			

3.3 Experimental validation and comparison of the models

Experimental data were compared with those obtained with the three models. Fig. 6 and Fig. 7 show the correlation of measured and simulated values for outlet air process temperature and air process humidity ratio. It can be observed that the experimental outlet air process variables of the DW was well predicted by the first and second order models, with R^2 greater than 97.4% for

outlet temperature and 95.1% for outlet humidity ratio for all 3 cases. The R^2 coefficients for ω_{po} obtained were lower than the R^2 coefficients for T_{po}.

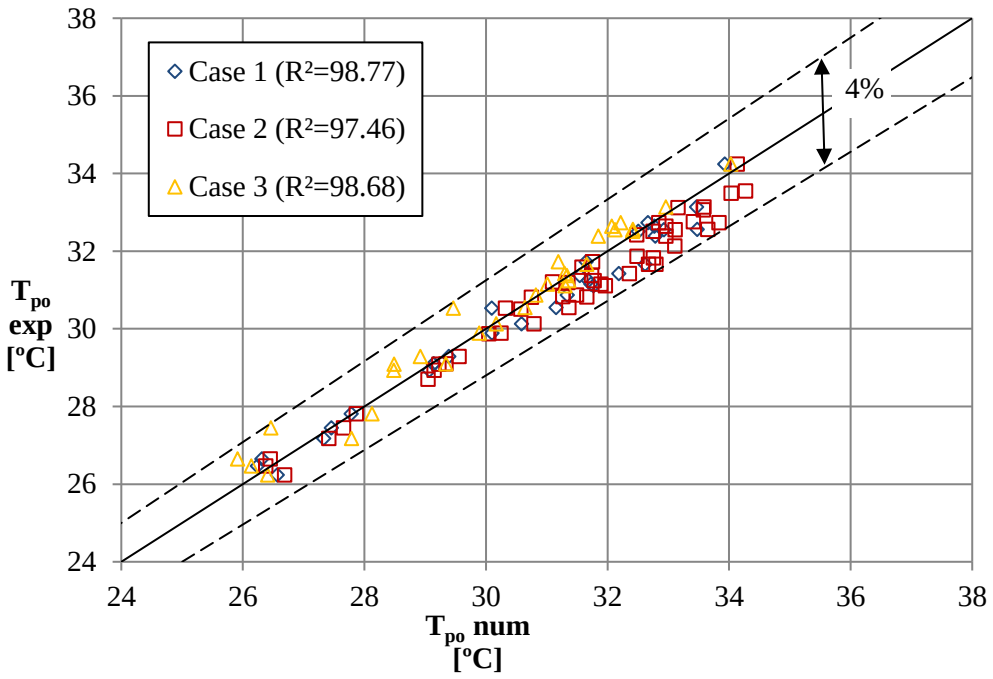

Fig. 6. Measured and simulated values for outlet process air temperature.

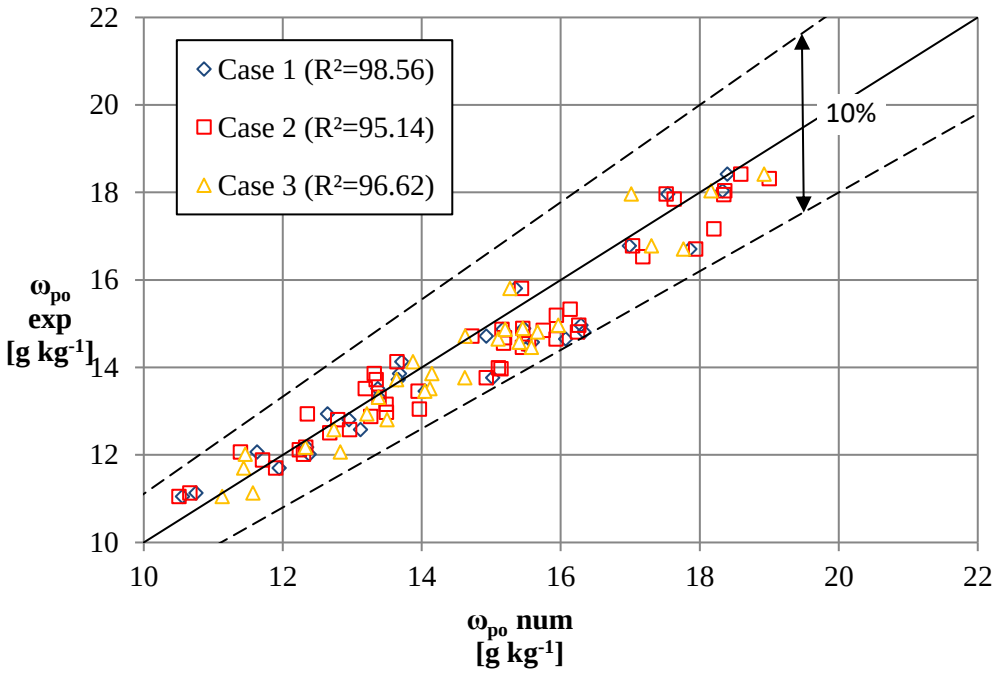

Fig. 7. Measured and simulated values for outlet process air humidity ratio.

The RMSE values and the maximum percentage deviation for the three models are presented in Table 9. The validation for case study 1 shows values within an acceptable level, with a number of design experimental tests of 19. The deviations and RMSE values were slightly higher in the case study 2 than in those obtained for case study 1. The slight loss of accuracy was caused by the increase of input variables. Finally, the case study 3 showed a slight improvement in accuracy, due to the additional inlet states to fit the model.

Table 9. Results of the tests of validation.

Model	N (design exp. tests)	Max $\|\delta T\|$ [%]	Max $\|\delta\omega\|$ [%]	$RMSE_T$ [ºC]	$RMSE_\omega$ [g kg^{-1}]
Case study 1	19	3.38	9.24	0.42	0.68
Case study 2	35	3.59	9.65	0.56	0.69
Case study 3	27	3.60	7.74	0.40	0.58

Therefore, the use of DOE methodology allowed to generate models of DW with a minimum number of tests with minimal temperature and humidity ratio deviations, below 4% and 10%, respectively. RMSE values were studied for the effectiveness method based on constant values [20], with a number of design experimental test of 107 and regeneration temperature range of 50-80°C. The $RMSE_T$ values predicted with the effectiveness method were greater than those obtained with the DOE methodology. RMSEω values were in very good agreement with those achieved with DOE methodology [20].

3.4 Response surfaces for case study 3

The main cross effects of the input variables on the output variables corresponding to the second order model, case study 3, are show in Fig. 8. It can be observed that T_{po} increased as T_{pi}, ω_{pi} and T_{ri} increased. However, an increase of ω_{ri} caused the opposite effect. It was also observed that an increase of T_{pi}, ω_{pi} and ω_{ri}, produced an increase of the value of ω_{po}. The opposite was true for variable T_{ri}. Similar results were obtained in [3,29].

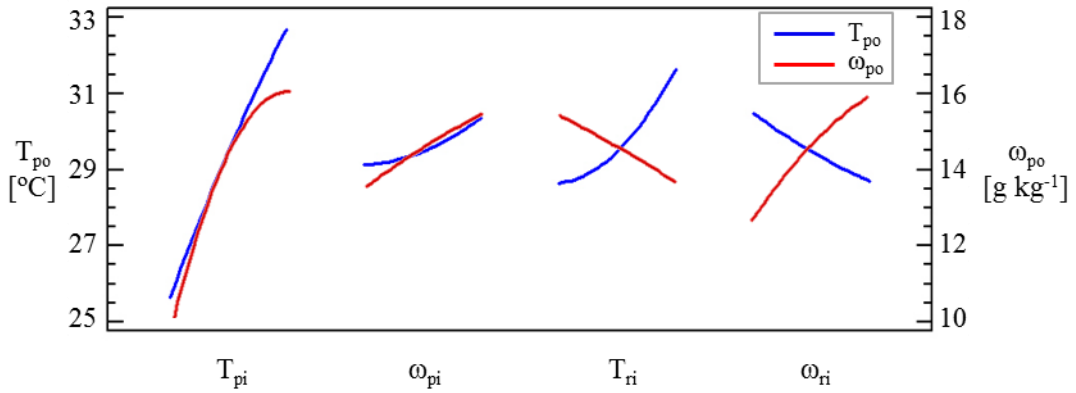

Fig. 8. Trends of the main cross effects for the temperature and humidity ratio of the process outlet air-stream for the case 3.

The response surfaces and contour line plots for outlet process temperature and outlet process humidity ratio were obtained from the second order model, corresponding to case study 3. T_{pi} and ω_{pi} were considered variables and T_{ri} and ω_{ri} were fixed at constant values of 40 °C and 15 g kg^{-1}, respectively. The trends of the treated air by the DW were similar for different values of T_{ri} and ω_{ri}, as shown in Fig. 9. It can be observed that T_{po} increased as T_{pi} was increased, when ω_{pi} remained constant. For example, an increase of approximately 1.5ºC for T_{pi}, yielded an increase of 1ºC for T_{po}. However, ω_{pi} exhibited a minimum variation of T_{po}, representing low gradient, when T_{pi} remained constant, see Fig. 9a and b. Regarding ω_{po}, low values were achieved when the inlet air was near saturation, i.e. for low values of T_{pi} and ω_{pi}. As ω_{pi} was higher, the outlet air process humidity ratio, ω_{po}, increased when T_{pi} remained constant, see Fig. 9c and d.

(a) Response surface for T_{po}	(b) Contour lines plot for T_{po}

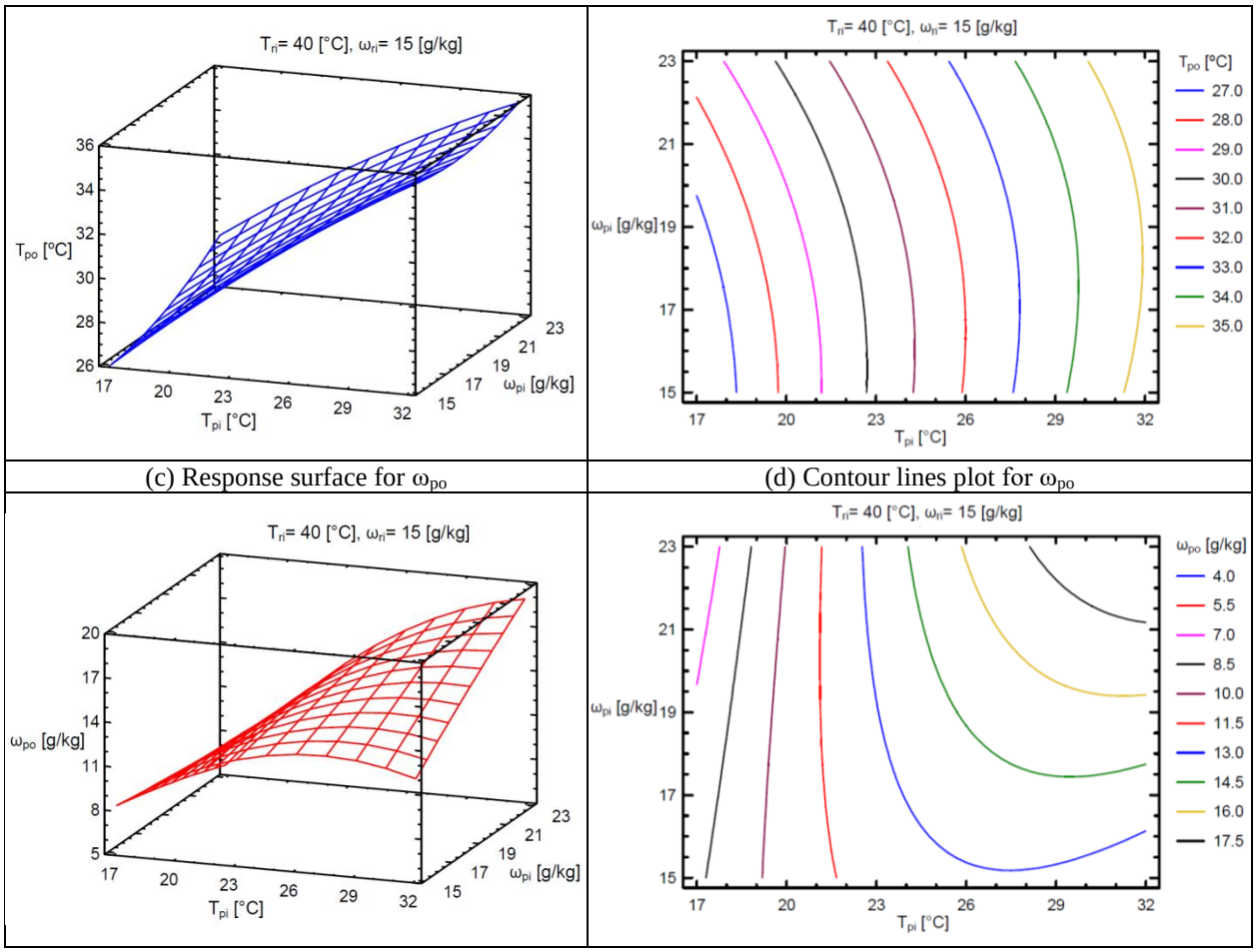

(c) Response surface for ω_{po} (d) Contour lines plot for ω_{po}

Fig. 9. Response surfaces and contour line plots for case 3 when the input variables T_{ri} and ω_{ri} remain constants.

Fig. 10 shows the response surfaces and contour line plots for outlet process temperature and outlet process humidity ratio, when T_{ri} and ω_{ri} were variables and T_{pi} and ω_{pi} were fixed at constant values of 23.5 °C and 18.5 g kg^{-1}, respectively. The trends of the treated air by the DW were similar for different values of T_{pi} and ω_{pi}. Regarding T_{po}, significant dependence on T_{ri} was observed, since a portion of regeneration heat was transferred to the process stream. However, the influence was reduced as T_{ri} decreased. Conversely, the influence of ω_{ri} on the output variable, T_{po} was weak, see Fig. 10a and b. The effect on ω_{po} was quite predictable. An increase of T_{ri} and a decrease of ω_{ri} resulted in a decrease of ω_{po}, see Fig. 10c and d. This effect was discussed in section 3.2.

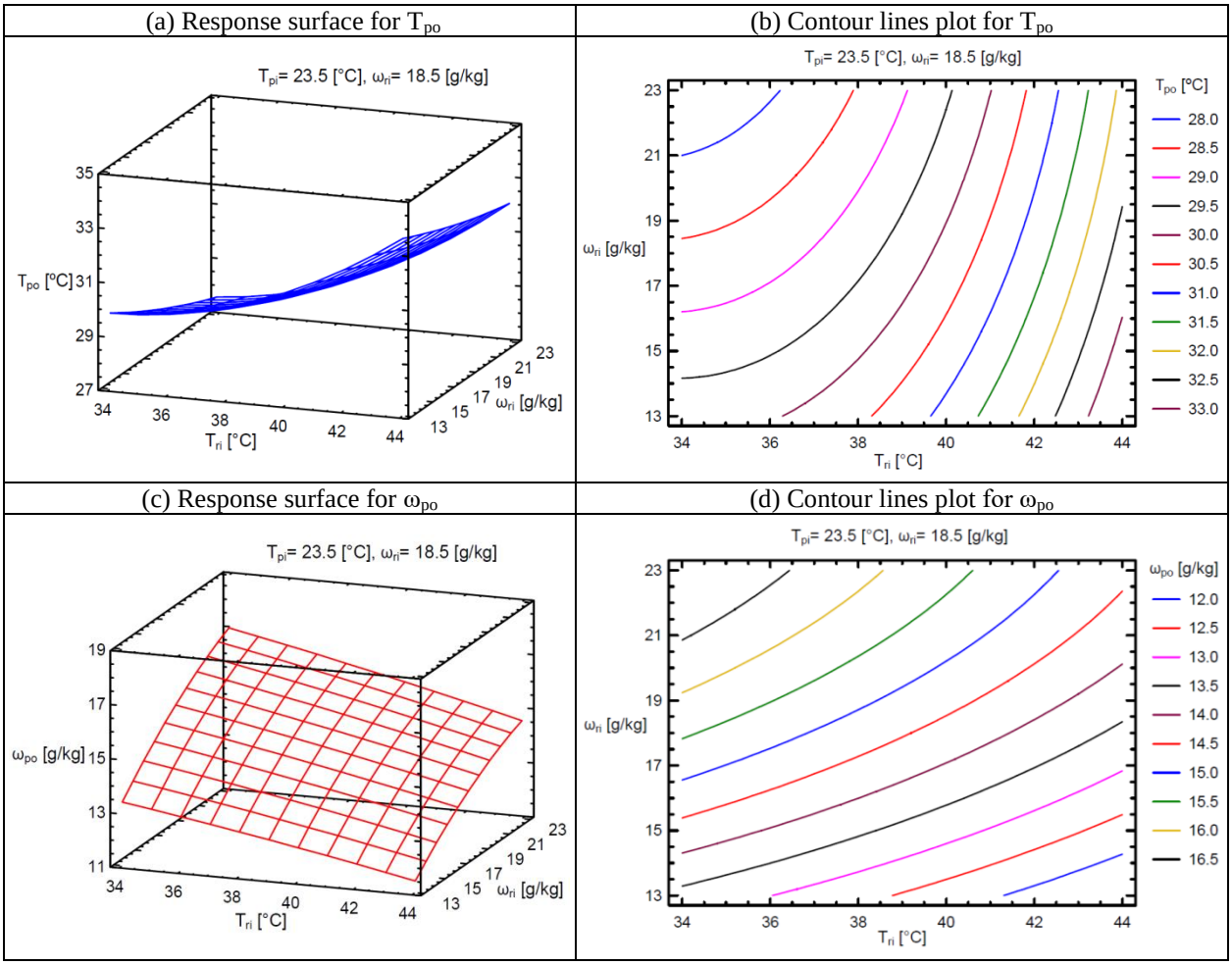

Fig. 10. Response surfaces and contour line plots for case 3 when the input variables T_{pi} and ω_{pi} remain constants.

4 CONCLUSIONS

In this work, three different numerical models of a DW were fitted using a methodology based on the statistical technique of design of experiments, DOE. The three mathematical models can be used to predict the air process outlet temperature and air process outlet humidity ratio in the DW especially for low regeneration temperature activated systems. Two first order models, case studies 1 and 2, and one second order model, case study 3, were fitted using experimental data. These three models considered the influence of the air inlet temperature and air inlet humidity ratio of the process and regeneration air on the DW. The influence of the process and regeneration airflow rate was also considered in the first order model for case study 2.

Experimental tests were carried out to fit the mathematical models 1, 2 and 3, in the range of low regeneration temperatures. A low number of experimental tests, 19, 35 and 27 respectively, were required.

The accuracy of the numerical results of the models has been found to be acceptable in all models, with maximum deviations below 4% for temperature and 10% humidity ratio. The second order model corresponding to case study 3 is considered the best option because of the balance between great accuracy of the model and low number of experimental tests.

The methodology of DOE has also allowed the identification of the most influential psychrometric factors in the behaviour of a DW. The results show a significant influence on the inlet humidity ratio of the air process and the air regeneration to achieve greater dehumidification.

The results suggested that the proposed approach was a valid methodology to study the global behaviour of a DW. It used a limited number of experimental tests and the simplified mathematical models obtained were suitable to be integrated in simulation tools.

Acknowledgements

Authors are grateful with the financial support provided by the Agency for Innovation and Development of Andalusia, expedient IDEA 360097, and by the Technological Corporation of Andalusia, expedient CTA 12/612, (2012-2014). This work is related to the research project Dehumidification and Air Drying, DESSECA, promoted by the company CIAT.

References

[1] Harriman III, L. Brundrett, G. Kittler, R. Humidity control design guide, American Society of Heating, Refrigerating, and Air Conditioning Engineers, Inc. (ASHRAE), 1791 Tullie Circle, N.E., Atlanta, GA 30329, 2001, 136–161.

[2] S.A. Mumma, J.W. Jeong, Direct digital temperature, humidity, and condensate control for a dedicated outdoor air-ceiling radiant cooling panel system, ASHRAE Transactions. 111 Part 1 (2005) 547–558.

[3] L.G. Harriman III, The dehumidification handbook, 2nd ed. , Munters Corporation, Amesbury, MA. (2003).

[4] Hines, A.J., T.K. Ghosh, S.K. Loyalka, and R.C. Warder, Jr. 1991. Investigation of co-sorption of gases and vapors as a means to enhance indoor air quality. ASHRAE Research Project 475-RP and Gas Research Institute Project GRI-90/0194. Gas Research Instit.

[5] A.G.C.C. American Gas Cooling Center. Applications Engineering Manual for Desiccant Systems, Arlington, 1996.

[6] K.F. Fong, T.T. Chow, C.K. Lee, Z. Lin, L.S. Chan, Advancement of solar desiccant cooling system for building use in subtropical Hong Kong, Energy and Buildings. 42 (2010) 2386–2399.

[7] M. El Hourani, K. Ghali, N. Ghaddar, Effective desiccant dehumidification system with two-stage evaporative cooling for hot and humid climates, Energy and Buildings. 68 (2014) 329–338.

[8] Y. Sheng, Y. Zhang, N. Deng, L. Fang, J. Nie, L. Ma, Experimental analysis on performance of high temperature heat pump and desiccant wheel system, Energy and Buildings. 66 (2013) 505–513.

[9] D. Kosar, Dehumidification System Enhancement, ASHRAE Journal. 48 (2006) 48–58.

[10] Y. Guan, Y. Zhang, Y. Sheng, X. Kong, S. Du, Feasibility and economic analysis of solid desiccant wheel used for dehumidification and preheating in blast furnace: A case study of steel plant, Nanjing, China, Applied Thermal Engineering. 81 (2015) 426–435.

[11] A. Al-Alili, Y. Hwang, R. Radermacher, A hybrid solar air conditioner: Experimental investigation, International Journal of Refrigeration. 39 (2014) 117–124.

[12] J.Y. San, S.C. Hsiau, Effect of axial solid heta-conduction and mass diffusion in a rotary heat and mass regenerator, International Journal of Heat and Mass Transfer. 36 (1993) 2051–2059.

[13] E. Vandenbulck, J.W. Mitchell, S.A. Klein, Design theory for rotary heat and mass exchangers .1. Wave analysis of rotary heat and mass exchangers with infinite transfer-coefficients, International Journal of Heat and Mass Transfer. 28 (1985) 1575–1586.

[14] E. Vandenbulck, J.W. Mitchell, S.A. Klein, Design theory for rotary heat and mass exchangers .2. Effectiveness-number-of-transfer-units method for rotary heat and mass exchangers, International Journal of Heat and Mass Transfer. 28 (1985) 1587–1595.

[15] C.R. Ruivo, J.J. Costa, A.R. Figueiredo, On the behaviour of hygroscopic wheels: Part I - channel modelling, International Journal of Heat and Mass Transfer. 50 (2007) 4812–4822.

[16] C.R. Ruivo, J.J. Costa, A.R. Figueiredo, On the behaviour of hygroscopic wheels: Part II - rotor performance, International Journal of Heat and Mass Transfer. 50 (2007) 4823–4832.

[17] Maclaine.Il, P.J. Banks, Coupled heat and mass-transfer in regenerators - prediction using an analogy with heat-transfer, International Journal of Heat and Mass Transfer. 15 (1972) 1225–1242.

[18] J.J. Jurinak, Open cycle desiccant cooling and Component models and system simulations, PhD thesis, University of Wisconsin, Madison, USA, 1982.

[19] G. Angrisani, C. Roselli, M. Sasso, Experimental validation of constant efficiency models for the subsystems of an unconventional desiccant-based Air Handling Unit and investigation of its performance, Applied Thermal Engineering. 33-34 (2012) 100–108.

[20] G. Panaras, E. Mathioulakis, V. Belessiotis, N. Kyriakis, Experimental validation of a simplified approach for a desiccant wheel model, Energy and Buildings. 42 (2010) 1719–1725.

[21] C.R. Ruivo, A. Carrillo-Andres, J.J. Costa, F. Dominguez-Munoz, A new approach to the effectiveness method for the simulation of desiccant wheels with variable inlet states and airflows rates, Applied Thermal Engineering. 58 (2013) 670–678.

[22] M. Beccali, F. Butera, R. Guanella, R.S. Adhikari, Simplified models for the performance evaluation of desiccant wheel dehumidification, International Journal of Energy Research. 27 (2003) 17–29.

[23] F.E. Nia, D. van Paassen, M.H. Saidi, Modeling and simulation of desiccant wheel for air conditioning, Energy and Buildings. 38 (2006) 1230–1239.

[24] F. Comino Montilla, M. Ruiz de Adana Santiago, A. Cerezuela Parish, M. Zamora García, F. Peci López, Design and building of a test facility for experimentation of desiccant wheels, in the Minutes Book of the National Congress engineering thermodynamics, Cartagena, (2015) 295–302.

[25] S. De Antonellis, M. Intini, C.M. Joppolo, F. Pedranzini, Experimental analysis and practical effectiveness correlations of enthalpy wheels, Energy and Buildings. 84 (2014) 316–323.

[26] M. Aprile, M. Motta, Grey-box modelling and in situ experimental identification of desiccant rotors, Applied Thermal Engineering. 51 (2013) 55–64.

[27] D.C. Montgomery, Design and analysis of experiments, 6th Edition, Wiley, 2004.

[28] Statgraphics Centurion XV, (2006). available from http://www.statgraphics.com/ (accessed 05.07.15).

[29] F.E. Nia, Sustainable Air Handling by Evaporation and Adsorption, PhD thesis, Deft University of Technology, 2011.